Original papers
Nanostructured, nanoscale materials and nanodevices

УДК 004+531-2+535+620-22 DOI: 10.17277/jamt-2025-10-04-329-341

Topological laser thermodynamics in technologies for controlling the functional characteristics of high-entropy alloys with dendritic surface structures

© Darya D. Tumarkina[a], Oleg Ya. Butkovsky[a], Dmitry N. Bukharov[a]✉, Irina V. Burakova[b], Alexander E. Burakov[b], Sergey M. Arakelian[a]

[a] *Vladimir State University, 87, Gorky St., Vladimir, 600000, Russian Federation,*
[b] *Tambov State Technical University, Bld. 2, 106/5, Sovetskaya St., Tambov, 392000, Russian Federation*

✉ buharovdn@gmail.com

Abstract: This paper examines the laser thermodynamics of topological structures – dendrites – obtained by laser ablation of several high-entropy alloys using laser pulses. Laser experimental synthesis schemes and parameters for producing dendritic structures in various high-entropy alloys are discussed. For various configurations of such structures, the possibilities for controlling the functional characteristics of dendritic samples (electrophysics and optics) for potential technological applications are analyzed within nanocluster/island topological models. Thermodynamic conditions for targeted dendritic synthesis are modeled and evaluated under various experimental conditions with laser irradiation from a Gaussian radiation source using the Matlab Laser Toolbox approximation. The thermodynamic conditions for the synthesis of dendritic systems formed from high-entropy alloys are studied using analytical estimates of the temperature field. The procedure performed allowed us to estimate the actual melting temperatures for the components of the nanostructured high-entropy alloy. Models of dendritic structures in the diffusion approximation under diffusion-limited aggregation were proposed. Their electrical conductivity was estimated using simulations of the current-voltage characteristics within the tunneling and hopping approximations, as well as the enhancement of the electric field on fractal structures at their inhomogeneous boundaries. The developed models were implemented in MATLAB and were directly related to the parameters of the actual synthesis scheme, and the estimates obtained using them were consistent with the actual values.

Keywords: laser thermodynamics; high-entropy alloys; topological surface structures; directed synthesis of dendrites; controlled functional characteristics.

For citation: Tumarkina DD, Butkovsky OYa, Bukharov DN, Burakova IV, Burakov AE, Arakelian SM. Topological laser thermodynamics in technologies for controlling the functional characteristics of high-entropy alloys with dendritic surface structures. *Journal of Advanced Materials and Technologies*. 2025;10(4):329-341. DOI: 10.17277/jamt-2025-10-04-329-341

Топологическая лазерная термодинамика в технологиях управления функциональными характеристиками высокоэнтропийных сплавов с поверхностными дендритными структурами

© Д. Д. Тумаркина[a], О. Я. Бутковский[a], Д. Н. Бухаров[a], И. В. Буракова[b], А. Е. Бураков[b], С. М. Аракелян[a]

[a] *Владимирский государственный университет имени Александра Григорьевича и Николая Григорьевича Столетовых, ул. Горького, 87, Владимир, 600000, Российская Федерация,*
[b] *Тамбовский государственный технический университет, ул. Советская, 106/5, пом. 2, Тамбов, 392000, Российская Федерация*

✉ buharovdn@gmail.com

Аннотация: Рассматривается лазерная термодинамика топологических структур – дендритов, полученных при воздействии лазерных импульсов на поверхность ряда высокоэнтропийных сплавов в процессе лазерной абляции. Рассмотрены схемы лазерного экспериментального синтеза и его параметры для получения дендритных структур

высокоэнтропийных сплавов различного характера. Для разных конфигураций таких структур в рамках нанокластерных/островковых топологических моделей проанализированы возможности управления функциональными характеристиками образцов с дендритами (электрофизика и оптика) для возможных технологических применений. Смоделированы и оценены термодинамические условия направленного синтеза дендритов при разных условиях эксперимента с лазерным воздействием от Гауссового источника излучения в рамках приближения Matlab Laser Toolbox. Проведено исследование особенностей термодинамических условий синтеза дендритных систем, образованных из высокоэнтропийных сплавов на основе аналитических оценок поля температуры. Проведенная процедура позволила оценить реальные температуры плавления для компонент наноструктурированного высокоэнтропийного сплава. Предложены модели дендритных структур в диффузионном приближении в рамках диффузионно-ограниченной агрегации, для которых приведена оценка их электропроводимости с помощью моделирования вольтамперных характеристик в рамках туннельного и прыжкового приближений, а также усиления электрического поля на неоднородных границах фрактальных структур. Разработанные модели реализованы в среде MATLAB и имеют непосредственную связь с параметрами реальной схемы синтеза. Оценки, выполненные с их помощью, не противоречат реальным величинам.

Ключевые слова: лазерная термодинамика; высокоэнтропийные сплавы; топологические поверхностные структуры; направленный синтез дендритов; управляемые функциональные характеристики.

Для цитирования: Tumarkina DD, Butkovsky OYa, Bukharov DN, Burakova IV, Burakov AE, Arakelian SM. Topological laser thermodynamics in technologies for controlling the functional characteristics of high-entropy alloys with dendritic surface structures. *Journal of Advanced Materials and Technologies*. 2025;10(4):329-341. DOI: 10.17277/jamt-2025-10-04-329-341

1. Introduction

The effect of laser radiation on the surface of a solid material is a multifactorial and controllable process under conditions of selected laser beam sizes and pulse durations, particularly when producing inhomogeneous dendritic surface structures.

This dimensional processing of the surface by laser radiation results in a topological modification of its structure under conditions of complex interactions between different phases of the substance during the development of nonlinear gas- and hydrodynamic processes with different spatiotemporal parameters, including micro- and nanoscale clusters. The emergence of such dynamic small-scale instabilities radically alters the thermodynamic phase and structural states of the medium, with parameters whose local values differ from those tabulated for bulk samples.

This specific feature of the laser experiment is of particular interest for complex/composite compounds, particularly high-entropy alloys (HEAs) of varying elemental/chemical composition [1, 2]. Precisely by applying laser radiation, it is possible to control the thermodynamic conditions for the formation of localized 3D columnar-dendritic structures of a fractal type, for example, on the metal surface of a sample, given the specific conditions of non-stationary energy exchange between light radiation, electronic states, and the lattice parameters of the solid. All this determines the final temperature regime and phase state of the medium with controlled functional characteristics.

This controlled laser radiation effect on a metal surface is particularly unique when applied in a sequence of laser pulses (multi-pulse mode). This allows for the selection of a specific time delay between pulses and the recording of the fundamental processes of sequential heating and cooling of the material, depending on the thermodynamic energy parameters of the alloy components, with specific melting conditions and the required deformation/pit configurations on the surface (including at the melting front). This also enables the time-lapse recording of the material's solidification conditions, including amorphization and crystallization processes, as well as oxidation under transient conditions.

Of fundamental importance in this case is the emerging localized thermophysical source, often moving in different regions on the material's surface. Its spatiotemporal characteristics require specialized analysis and modeling to ultimately produce a stable structure with the desired functional and structural properties of a 2D thin-film system of varying thickness.

Under conditions where the laser beam is scanned across the surface, dendrites in the melted zone form at a certain angle to the sample surface due to an additional temperature gradient along the direction of the laser beam's movement across the surface. Physical significance, in terms of thermal heating, is typically derived from a dimensionless control parameter such as the product of the laser focal spot size on the surface of the metal alloy and its absorptivity.

These issues are addressed in this paper for HEA of different chemical composition with a laser-induced dendritic structure. Emphasis is placed on the

fractal nature of the resulting configurations in terms of the thermodynamic and thermophysical processes that drive their development, along with the corresponding energy potentials for mixing thermodynamic quantities for alloys (in particular, entropy and enthalpy). This ultimately determines the structural and functional characteristics of samples with such synthesized surface topological structures. To analyze these characteristics, depending on the specific experimental conditions of the laser experiment, the authors conduct numerical modeling of the thermophysical processes that lead to various similar structural configurations on the surface.

2. Methods and approaches

This section briefly discusses schemes for obtaining a number of topological configurations that arise on the surface of a material under the influence of laser beams, and simple models of the electrophysical characteristics of such structures.

2.1. Laser action on the surface of a material and analysis of the implementation of inhomogeneous structures of the dendritic/fractal type on it

Initially, solid-phase laser modification of the surface of various metal-containing materials occurs under the influence of laser radiation. However, this laser ablation process occurs over a relatively narrow range of laser power values. Therefore, to determine the upper energy limit, above which melting of the sample is observed, we simulated the metal sample while scanning the laser beam. This allows us to subsequently calculate the configuration and composition of the resulting spatially distributed structure at the end of laser surface modification.

Since in typical cases for a metal surface the thermal diffusion length (~1 mm) ($l_d \sim \sqrt{D\,\tau}$, $D \sim 10^{-5}$ $\mathrm{m^2 s^{-1}}$ is thermal diffusion coefficient, $\tau \sim 0.1$ s is exposure time, then $l_d \sim 10^{-3}$ m) along the normal to the surface during the exposure time of the laser beam is much greater than the absorption length of the laser radiation (~10 μm), then the heat source can be considered superficial, which determines the direction of heat flow from this source.

A model of the laser heating process under conditions of surface film formation has been considered in many papers [1, 2]. The authors used calculations in the Matlab environment using library functions implemented in Matlab Laser Toolbox [3]. The intensity distribution $I(x, y)$ of laser radiation in the form of a Gaussian beam on the plane of the irradiated film (XOY) was specified as:

$$I(x,y) = \frac{8P}{\pi d_f^2} \exp\left[-\left(\frac{2\sqrt{2}}{d_f} \right)^2 \left(x^2 + y^2 \right) \right], \qquad (1)$$

where P is laser radiation power, W; d_f is beam diameter at the target surface, m.

The temperature field $T(x, y)$ of a moving surface heat source (its current coordinates are marked with a prime) in the quasi-stationary case can be represented as:

$$T(x,y) = \int_{-\infty}^{\infty} \int AI(x',y') W(x,y,x',v)\, dx'dy', \qquad (2)$$

where $W(x,y,x',v) = \frac{1}{2\pi KR} \exp\left(-\frac{v}{2a}(x - x' + R) \right)$, and $R = \sqrt{x^2 + y^2}$, A – absorption capacity in a material, K is thermal conductivity, $\mathrm{W \cdot (m \cdot K)^{-1}}$, $a = K/\rho c_p$ is thermal diffusivity, $\mathrm{m^2 \cdot s^{-1}}$, v is scanning speed, $\mathrm{m \cdot s^{-1}}$, ρ is medium density, $\mathrm{kg \cdot m^{-3}}$ and c_p is specific heat capacity of the material, $\mathrm{J \cdot (kg \cdot K)^{-1}}$.

Expression (2) is calculated, for example, using the fast Fourier transform [4].

Using expressions (1) and (2), we calculated the temperature field distribution on the target surface (the specific chemical composition of the HEA is shown below in Fig. 1) in a square, flat computational domain measuring 400 μm. These calculations allowed us to establish an upper limit for the laser power beyond which sample melting occurs. At laser power levels of no more than 10 W, the maximum calculated temperature field values did not exceed the numerical values for melting to occur, i.e., surface deformation – in our case, nanomodification – occurred.

In order to study the physics of the processes occurring during such laser modification of the surface, detailed experiments were previously carried out with well-studied materials, the processes in which can be considered as test ones within the framework of an analogy for the case of HEA materials studied by us in this article: semiconductors, in particular, lead telluride, PbTe [5]; metallic ones, in particular, from the noble metals silver Ag, gold Au and their alloys [6]; metal-carbon and diamond-like compounds of different compositions [7–9]. In this case, the emphasis is placed on various schemes and modes of laser modification of the surface with controlled synthesis

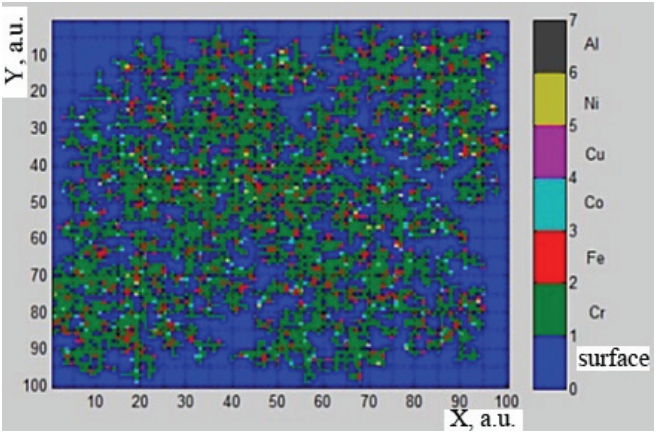

Fig. 1. Representative image of HEA dendritic nanostructures, with their chemical composition depicted by different colors (in relative units)

of topological cluster structures of a certain fractal-type configuration in thin-layer systems on a solid surface. Modeling of the occurring thermal diffusion processes and the implementation of inhomogeneous topological structures of different configurations on the surface of the material are possible using solutions of the two-dimensional diffusion equation [10].

Since, in principle, such methods and approaches for synthesizing such heterogeneous and disordered structures are quite universal, they are also feasible for our problem of HEA with dendrite formation, at least during the initial stage of exposure to a laser pulse with a specific time profile. Basic approaches for such consideration are provided in (Supplementary materials 1).

A typical view of the dendritic microstructure we obtained for HEA is shown in Fig. 1, which shows an image of the dendritic configuration taking into account the HEA elemental composition (shown on the scale on the right in the figure, with the corresponding color). This composition was determined using X-ray microanalysis. The image is given in relative units, taking into account model processing of the image.

We previously considered a number of examples of model heterogeneous nanostructures [8, 9] using certain parameters, including fractal dimension, and taking into account the height of the formed dendrites, which were also recorded in the AFM imaging experiment.

These models allow us to estimate the sizes of the formed dendrites. Converting to absolute sizes, taking into account the 10 nm side length of the computational domain cell, we obtain minimum coverage circle radii for the bases of the formed dendritic clusters in the order of 100–400 nm.

The dimensions of the crystallized metal blocks after laser ablation are several tens of nanometers, which is an order of magnitude smaller than the inhomogeneities in the original sample. The cladding processes for a pre-applied alloy coating to the sample surface, followed by its solidification after rapid cooling, are not considered here. It can be argued that the formation of high-energy electron transport dendrites on the surface of, for example, stainless steel, is an adiabatic thermodynamic process of their synthesis [10]. Dendrites are precursors to the formation of crystalline structures.

2.2. Electrical conductivity models

Existing approaches to assessing the functional characteristics of this type of dendritic structure, in particular, models of electrical conductivity of disordered structures, which include nanocluster/ island surfaces with nanoclusters, are determined by the surface structure and its dendritic features. In general, to assess the electrical properties of heterogeneous structures of various configurations – nanocluster/island films/dendrites with disconnected topology, where there is no continuous conductivity path – the electric current between adjacent nanoclusters is considered. Within this approach, nanoclusters/islands are represented as potential wells, and the spaces between them act as potential barriers [11].

The emission of charge carriers into the surrounding medium or onto the substrate itself, as well as direct or hopping electron tunneling, forms the mechanism for charge transfer between nanoclusters of different configurations located on a solid surface.

Isolating the conductivity path in such a structure within the framework of the applied approach [12] allows us to evaluate the current-voltage (I–V) characteristics of the system (the dependence of current I on voltage U).

Depending on their topological features, such surface cluster structures with dendrites can be divided into two types of samples: those with a fairly dense arrangement of dendrites and those with a sparse structure.

In the first type of samples, topological clusters are connected to each other by "bridges," forming a connected topology that allows for the identification of a continuous current path with percolation-type electrical conductivity [5]. The I–V characteristic for this case is calculated using the standard relation (Ohm's law).

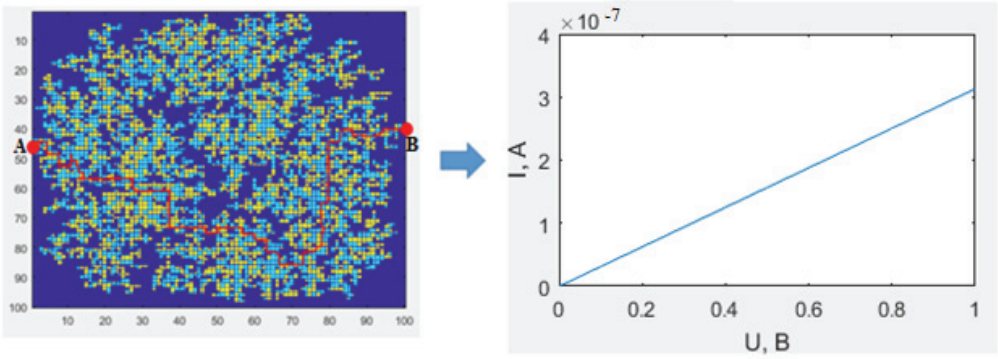

(a) *(b)*

Fig. 2. Model of a HEA film with a highlighted conductivity path *AB* (*a*);
I–V characteristics of the film for path *AB* with a test grain size of 10 nm (*b*)

The second type of samples possess fairly large distances between nanoclusters/islands and can be characterized by dielectric conductivity mechanisms, in which the electrical conductivity cluster forms a disconnected set, resulting in the absence of a continuous current path, and hopping electrical conductivity mechanisms in various manifestations [7, 11].

For these cases, mathematical modeling of the electrophysical properties of such dendritic structures is well known and has also been performed by the authors [8, 12]. The general scheme of such a process is based on DLA (diffusion-limited aggregation) modeling for percolation-type electrical conductivity [8, 10].

Figure 2 shows a model of a nanocluster/island HEA-nanofilm possessing this percolation type of conductivity, with a distinguished conductivity path and the corresponding I–V characteristic. The structure (Fig. 2*a*) was modeled on a computational domain of 100×100 relative units, within the framework of the DLA model, with a value of the probability of adhesion (*s*) of particles during their agglomeration equal to 0.5, and a random initial distribution of 10 seed particles at an equal concentration of HEA elements. In the film structure, specified points of microcontacts for voltage application (*A* and *B* points) are distinguished. Using the Lee wave algorithm [9, 12, 13], a continuous conductivity path is realized, taken as the shortest trajectory of electron motion in the nanofilm (*AB* broken line), the length of which *L* is 163 relative units. To calculate the current-voltage characteristics in test model units, the size of the structure granule corresponding to the cell size of the calculation region was chosen equal to d_{m1} = 10 nm.

Thus, hopping conductivity is realized as a process of charge carrier transport through localized centers [7, 13].

For a random distribution of localization centers, the electrical resistance R_{03} takes the form [14, 15]:

$$R_{03} = \frac{\pi\hbar a}{3.84q^2}\exp\left(\frac{1.24}{aN^{1/3}}\right), \qquad (3)$$

where N is concentration of localization centers m^{-3}, q is electron charge C, $\hbar$ is reduced Planck constant.

In connection with this approach (its basic principles are analyzed in (Supplementary materials 2), it is useful to briefly examine the model of electric field amplification in fractal structures such as those shown in Figs. 1 and 2*a*. As can be seen, in their simplest model representation, they include arbitrarily oriented elements in the form of variously sized fragments of long branches with fractal segments at their ends.

Thus, this analysis demonstrates that, using model samples and the proposed approximation, it is possible to achieve a relative enhancement of the electric field by several orders of magnitude, taking into account the entire perimeter of the branched fractal figure in a specific region of the coating when measured with a certain cross-section of the microcontact end. This effect is analogous to the well-known phenomenon of the realization of supersonic Raman scattering (SERS) with enhancement on a rough surface, used, in particular, in the diagnostics of extremely low concentrations of dyes on such surfaces [11, 16–18].

3. Results and Discussion

3.1. General characteristics of thermophysical laser action in the experiment

When using laser heating in HEA, it is necessary to consider the specific nonlinear temperature dependence of the material's characteristics and the microstructure of the resulting objects. This is the

subject of separate research, particularly in terms of potential applications, which is beyond the scope of this article.

This section presents the calculation results for processes in an HEA system under laser irradiation of the material surface, using fairly universal fundamental approaches to the thermodynamic description of laser heating. We also analyze some aspects of the conditions for the formation of inhomogeneous structures on the surface of samples in the corresponding temperature ranges under laser irradiation of materials (if necessary, these conditions can be adjusted for the specific elemental composition of the HEA in different schemes).

We will take into account the technologically important multi-pulse nature of radiation with a repetition rate of laser pulses f in the form of a simple dependence:

$$I(t) = I_0(t)(1-\cos f t),$$

where $I_0(t)$ is a slowly changing function over time, taking into account the difference in amplitudes in the sequence of pulses/peaks of different origin in each pulse [1, 2, 19, 20].

Then, in the one-dimensional approximation of the propagation of the thermal field along the *OX* axis in the quasi-stationary case, when the current value of t is considered within the general envelope of the laser pulse duration, for the temperature T we have [20]:

$$T(x,t) = \left(\frac{2w_0\sqrt{\beta t}}{a}\right)\mathrm{ierfc}\left[\frac{x}{2\sqrt{\beta t}}\right], \qquad (4)$$

w_0 is energy density of laser radiation flux, J·m^{-3}; β is thermal diffusivity coefficient, $\beta = a/(c\rho)$ m^2·s^{-1}; a is thermal conductivity, W·(m·K)$^{-1}$; ρ is density, kg·m^{-3}; c is specific heat capacity, J·(kg·K)$^{-1}$; and parameter

$$\mathrm{ierfc} = \int_z^\infty \mathrm{erf}\, c(z)dz = \left(\frac{1}{\pi^{1/2}}\right)\mathrm{e}^{-z^2} - z\ \mathrm{erfc}(z)$$

is the integral of the probability integral function. It is assumed that the radius of the laser heating spot focused on the material, r_f is much greater than the spatial scale of thermal diffusivity, β, for the time being considered, t .

The paper examines dendrite growth perpendicular to the sample surface, and the parameter x determines its height.

For example, an estimate for iron yields a value of x ~50 μm.

On the surface of a thin plate $x = 0$, i.e. when its thickness h is much smaller than the radial dimensions of the laser heating region under consideration $r = r_f$ and under the condition that $t \le 0.2 r_f^2/\beta$, instead of expression (4) we have a simpler relationship:

$$T(0,t) = \frac{\left(\frac{w_0 t}{ch}\right)(1-4\beta t)}{r_f^2}\exp\left(-\frac{r_f^2}{4}\beta t\right). \qquad (5)$$

The analysis of the problem shows that the maximum heating temperature depends on two dimensionless parameters: a nonlinear function of temperature and the material's density. Moreover, for short periods of time, i.e., at the onset of the laser pulse, the temperature field in the material is determined by the energy flux density distribution function w_0 on the sample surface, for which the result of the one-dimensional heating problem with a constant heat source, multiplied by the value of w_0, is applicable.

The fundamental parameter in the problem under consideration is the required value of the laser radiation flux density q, at which the maximum temperature $T_{\max}$ is reached on the sample surface by the end of the laser pulse and at which melting of the material occurs. Without dwelling on the corresponding analytical relations (these processes are considered, for example, in [21]), we will immediately present numerical estimates of the critical values q_c based on these relations for the onset of melting of the material at normal pressure. In particular, for steel (SHX-15) with thermal conductivity $\alpha = 0.51$ W·(cm·K)$^{-1}$, volumetric heat capacity $c = 0.15$ cm^2·s^{-1}, $q_c = 3.5\cdot10^3$ W·cm^{-2} we have achieved the value $T_{\max} = 1808$ K with a laser pulse duration of 1 ms. With a duration of 10^{-8} s the required value q_c for melting the material $q_c = 1.8\cdot10^5$ W·cm^{-2}.

In this case, q_c increases for different materials with increasing melting point, thermal conductivity, and specific heat capacity. However, the q_c value decreases with increasing laser pulse duration. For example, for titanium, $T_{\max} = 2073$ K, $a = 0.15$ W·(cm·K)$^{-1}$, $c = 0.06$ cm^2·s^{-1}. For the noted laser pulse durations of 1 ms and 10^{-8} s, we have q_c, values of $3.0\cdot10^3$ W·cm^{-2} and $1.0\cdot10^5$ W·cm^{-2}, respectively.

When considering the rate of movement of temperature phase transition boundaries (along the

time coordinate), which determine dendrite growth, in this non-stationary problem, the region where exponential growth toward a fixed value of a given melting temperature is of fundamental importance.

However, during multi-pulse laser irradiation of a material, for example, for a pair of successive pulses, two parameters must be evaluated: the heating rate from the first pulse and the subsequent cooling of the material until the arrival of the second pulse, with a certain time delay δt (Supplementary materials 1). Then, according to the physics of the phenomenon under consideration, the heating and subsequent cooling of the material from the first pulse is limited in time by the arrival of the next pulse with a selectable delay δt, which determines the role of the time duration t of the dendrite growth process under the influence of the first pulse.

Thus, it becomes possible to regulate the modes of thermophysical processes during multi-pulse exposure of laser radiation to materials with controlled production of different dendritic configurations over time, and this can also be done in different areas of the surface with a given scanning of the laser beam over the surface.

3.2. Features of HEA systems

The above discussion applies to a material with a homogeneous elemental composition. Therefore, for HEA, a comprehensive analysis must be conducted, taking into account thermal diffusion effects for the various chemical components of the alloy. It also takes into account that the maximum laser heating temperature shifts toward a less thermally conductive material to a greater extent the longer the laser pulse duration [10, 20].

We consider several of the obtained dependencies within the framework of the general approach outlined above. In doing so, we will significantly simplify the problem for the case of only two consecutive laser pulses with specific characteristics acting on the HEA (with the formation of dendrites).

In this model, we will assume that laser radiation induces two layers in depth with defined boundaries, taking into account the sequential heating and cooling processes [22]. The first layer (with an average thickness of about 1 μm) has a columnar-dendritic structure, mainly of martensite; the second has a fine-grained structure with retained austenite (with average grain sizes of up to twenty micrometers and a temperature gradient across the depth of the laser-impact zone of the order of several tens of micrometers). Their characteristics are determined by the rates of amorphization, crystallization, and heat-diffusion processes in the material for different HEA components, as well as by the laser irradiation modes with a time interval between two successive pulses.

Furthermore, when exposed to millisecond-duration laser pulses in an air atmosphere, metal oxidation processes occur (with oxide film thicknesses of up to fractions of a micrometer). The kinetics of metal oxidation depends on the thermal effect of laser radiation integrally (on a two-component system), taking into account the growth of the oxide component. These phenomena are well known in materials science [23, 24], but are discussed below with corresponding numerical estimates for a specific HEA composition.

The subject of the study is HEA with chemical elements in AISI 304 stainless steel, with their percentage concentrations presented in Table 1 [25], before laser irradiation. A series of experiments were conducted with this material under double-pulse irradiation in the non-uniform laser pulse (M-pulse) model [22]. This multicomponent material decomposes at a temperature of 1067 K. However, here we are specifically talking about HEA-type alloy, since it requires comparable concentrations of its constituent chemical elements.

According to [22], on such a substrate, where HEA is located, the areas of formation of dendrites with their most uniform distribution over the surface are realized in the temperature range [608–800 K].

Our analysis of the scheme of this two-pulse action on the material led to the results presented in Table 2 and in Figs. 3 and 4 for the selected parameters of the laser experiment.

Using Matlab, the authors obtained a temperature distribution field on a stainless steel substrate under parabolic growth conditions (Fig. 5).

Table 1. Concentrations of chemical elements (wt. %) in stainless steel AISI 304

C	Cr	Ni	Si	Mn	S	P	N
0.08	18–20	8–10.5	1	2	<0.03	0.045	0.06

Table 2. Temperature of the substrate with formed HEA (stainless steel) depending on the time of exposure to 2-pulse laser ablation

t, ms	0	3/2	3	9/2	6
$T(t)$, °C	300	469	433	506	300

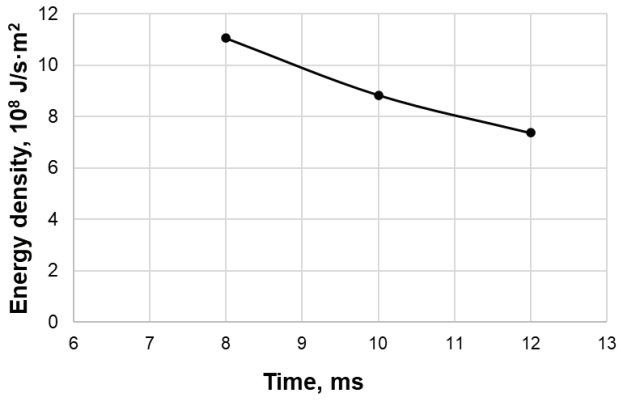

Fig. 3. Dependence of the laser energy density acting on the sample on the exposure time as a result of 2x ablation on the surface of a stainless steel substrate with formed HEA

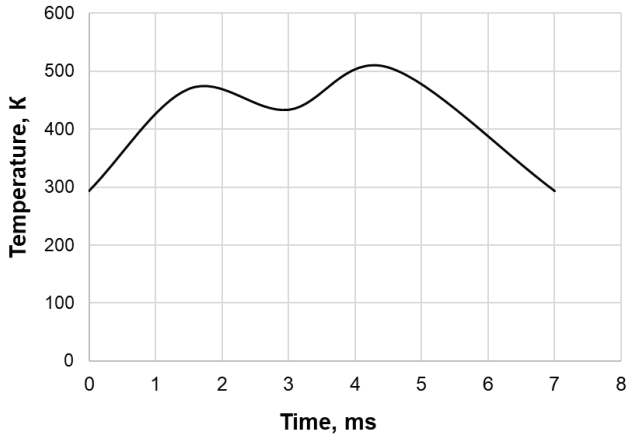

Fig. 4. Dependence of the temperature of the stainless steel substrate with the formed HEA on the total time of exposure to two laser ablation pulses

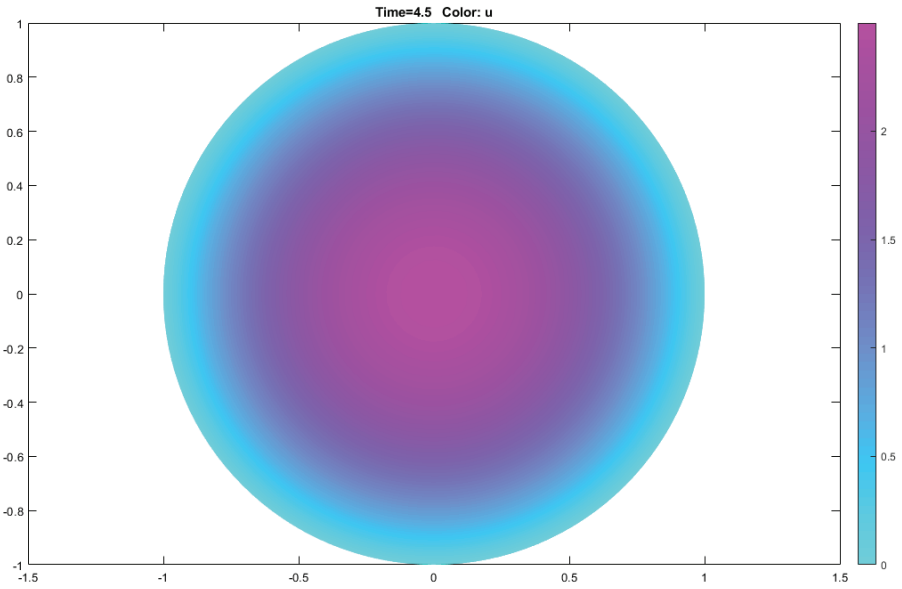

Fig. 5. Temperature field on a stainless steel substrate with HEA formed as a result of 2-pulse ablation. Calculations were performed in Matlab; with an exposure time of 1 ms, a temperature of 335 °C is reached; with an exposure time of 1.5 ms, this corresponds to 608 °C; with an exposure time of 3 ms, this corresponds to 964 °C

The initial conditions for the calculation were the initial and final temperatures of the laser exposure, and the total exposure time intervals (on the left side of the figure) were 1, 1.5, 3 ms (shown in different colors on the right scale).

In the above-described two-pulse laser irradiation scheme, the concentration of each HEA impurity was calculated for the temperature gradient formed during the second pulse, and the melting temperature of each impurity was also calculated. This can be accomplished using Fick's second law [10, 20, 24]:

$$\frac{C_x}{C_0} = 1 - \mathrm{erf}\frac{x}{2\sqrt{D\tau}}, \qquad (6)$$

where C is concentration of diffusing substance in a film with thickness x, m^{-3}; C_0 is initial concentration of the diffusing substance in the liquid, m^{-3}; erf is error function with tabulated values [26]; x is layer thickness, m; D is diffusion coefficient, $m^2 \cdot s^{-1}$; τ is diffusion time, s. This makes it possible to calculate the concentration of impurities after exposure to the first laser pulse.

Diffusion coefficient values D in HEA for each ion (Cr^+, Ni^+, Mn^+, C^+, Fe^+) are tabulated [20] and are equal to: $D(Cr^+) = 0.01 \cdot 10^{-4}$ $m^2 \cdot s^{-1}$; $D(Ni^+) = 21.9 \cdot 10^{-4}$ $m^2 \cdot s^{-1}$; $D(Mn^+) = 7.5 \cdot 10^{-4}$ $m^2 \cdot s^{-1}$; $D(C^+) = 0.33 \cdot 10^{-4}$ $m^2 \cdot s^{-1}$; $D(Fe^+) = 0.0062 \cdot 10^{-4}$ $m^2 \cdot s^{-1}$.

Given the processes of laser oxidation, the dependence of the thickness $h(r, t)$ of the oxide film on the temperature on the surface of stainless steel was obtained under the assumption of a parabolic law of its growth [23, 24, 27]:

$$h(r,t) = \sqrt{2t\omega_0(-Q/T(r))}, \quad (7)$$

where $h(r, t)$ is film thickness, m; t is laser pulse duration, s; r is transverse coordinate, m; Q is oxidation activation temperature, equal to approximately 1143 K; $T(r)$ is maximum heating temperature, K; ω_0 is parabolic constant of the oxidation growth rate, which under dry oxygen conditions at temperature ~1100 K is equal to 0.027 $\mu m^2 \cdot h^{-1}$ [23, 24].

Thus, at a stainless steel surface temperature of 1860 K and a laser pulse duration of 6 ms, the oxide film thickness is 0.7 nm.

The melting point of the stainless steel components involved in dendrite formation was also calculated.

According to [28–30], difference in chemical potentials of components is $\Delta\mu = -q(T_0 - T)/T_0$, where T_0 is melting point of the components, K; T is phase transition temperature. According to [22, 31] it equals to 1067 K, and we have that $q = \frac{\sum \mu_i n_i}{T}$ is latent heat of phase transition, where is concentration of the i-th component of HEA. Taking into account each concentration n_i the HEA component: $\sum n_i = \frac{k}{s} \rho S_{surf}$, where k is Boltzmann constant, $J \cdot K^{-1}$; S is surface entropy, $J \cdot (K \cdot m)^{-2}$; ρ is dendrite distribution density, m^{-2}; S_{surf} is surface area, m^2.

On the other hand, $\Delta\mu$ is an additive quantity, therefore $\Delta\mu_i = \mu_{li} - \mu_{si} = q(T_0 - T)/T_0$ is the difference in chemical potentials of the i-th component, which is equal to the difference in chemical potentials for the liquid and solid states of the component, T_i is melting point of the component, K. In this case $\sum \mu_i n_i = \Delta G$ [30], where G is the Gibbs free energy unit, J. Therefore, we arrive at the expression [31]: $q\frac{T_0 - T}{T_0 T R} = \frac{1}{n}$, where n is the number of particles of a given component.

Let us consider the concentrations of the HEA components in the oxide film [23, 24].

For the differential $d\gamma$ from the surface tension of a flat surface, we have according to [30]:

$$d\gamma = -M_1 d\mu_1 - M_2 d\mu_2 - \ldots - M_6 d\mu_6,$$

where M_i is the excess number of moles of the i-th component ($i = 1, \ldots, 6$) per unit area of the interfacial layer.

Then we write:

$$x_1 d\mu_1 + x_2 d\mu_2 + x_3 d\mu_3 + x_4 d\mu_4 + x_5 d\mu_5 + x_6 d\mu_6 = 0,$$

where x_i is molar fractions of components.

Thus, for a separate (in particular) component $i = 6$, we have

$$d\gamma = \left[M_6 - \frac{x_6}{x_1 M_1 + x_2 M_2 + x_3 M_3 + x_4 M_4 + x_5 M_5} \right] d\mu_6$$

or, introducing the appropriate notation, we have $d\gamma = M_{6(12345)} d\mu_6 = M_{6(12345)} R T\, d \ln c_6$, where R is universal gas constant, $J \cdot (mol \cdot K)^{-1}$; T is the melting point of the 6th component K; c_6 is the concentration of the 6th component, m^{-1}.

Similar equations are valid for all components. Since the alloy is equimolar (high-entropy), we assume that $M_1 = M_2 = \ldots = M_6$. However, in HEA, the proportions of each component range from 0.05 to 0.3, depending on the total number of components – N. This corresponds to the generally accepted concept of HEA and can be a controlling parameter, along with chemical composition and concentrations, in the synthesis of specific HEA.

From here, for $d\mu_i$ we obtain:

$$d\mu_i = \frac{\Delta G_i}{n_i} = RT \ln \frac{n s}{k}. \quad (8)$$

In this case, if we consider the thermal decomposition reaction as endothermic, we can determine the amount of heat required for melting each impurity, taking into account the heat input from laser heating and melting. We will express this in terms of temperature based on the relationship between the concentrations of substances in the liquid layer:

$$n = \frac{R T_0 T}{q(T_0 - T)}.$$

Then from [30–32]:

$$\frac{\Delta G_i (T_0 - T)}{T_0 T} = RT d \ln \frac{T_0 T}{T_0 - T}.$$

Now we can find the melting temperatures of the particles for the HEA elements of interest to us (Cr, Ni, Mn, C, Fe).

Let us assume that as a result of oxidative destruction, an atomic monolayer of impurities is formed on the surface of stainless steel. Then, from the phenomenological thermodynamic model for describing the melting temperature of nanoparticles of materials [32], we obtain the following two expressions

$$4\pi\left(\frac{\delta}{2}\right)^2 d = \frac{4}{3}\pi\left(\frac{\delta}{2}\right)^3, \quad (9)$$

where δ is Tolman's constant, m; d is atomic monolayer height, m;

$$T_m = T_m^{(\infty)} \exp\left(-\frac{4\delta}{\delta + 2R}\right), \quad (10)$$

where $T_m^{(\infty)}$ is melting point of a bulk sample, K; r_0 is radius of a particle/cluster (in our case, an atom), m.

The obtained melting temperatures of massive samples $T_m^{(\infty)}$ [30, 32] and the atomic radii$r_0$of metals are given in Table 3 [33].

Using the data from Table 3, we obtain the calculated values of the melting temperatures T_m, but for the nanoparticles of the HEA components. This gives the following numerical values: for C – 129 K, for Cr – 90 K, for Fe – 74 K, for Ni – 74 K, for Mn – 64 K. For different HEA elements, we have the following values of n: 0.13 for C; 0.09 for Cr; 0.07 for Fe; 0.07 for Ni; 0.06 for Mn.

Thus, using the proposed approach, it is possible to estimate the actual melting temperatures of the components of nanostructured HEA. This will determine their potential use in various applications for specific purposes.

Table 3. Data on the melting temperature of massive samples T_m for HEA of the elemental composition under consideration

Chemical element	$T_m^{(\infty)}$, K	r_0, nm
C	3800	0.091
Cr	2150	0.130
Fe	1806	0.126
Ni	1725.4	0.135
Mn	1517	0.132
O	1860	0.386

3.3. Prospects and background for the application of nanostructured HEAs

Such high-entropy perovskites of the dendritic fractal type hold great promise for various applications, particularly in electrophysics.

According to the physics of the phenomenon itself, the reduction of a metal (stainless steel) from a perovskite modeled on experimental data results in the formation of an oxide film on the dendrite surface. Upon reduction, this perovskite transforms into a martensite structure. This occurs due to the interaction of the perovskite (essentially an ore [34]) with atmospheric carbon monoxide. This assumption is based on the fact that the carbon content in the crystal lattice increases. Moreover, according to the same work [34], the charge in the oxide lattice is compensated, so there are no free electrons in the oxide lattice, and charge transfer within the lattice is carried out only by ionic displacements. With a change in the structure of the electric field in the medium, only paired, and therefore neutral, thermal objects are formed in the ionic lattice of the perovskite – interstitial defects and Frenkel defects, or Schottky defects. Therefore, the electrical conductivity of such a lattice is due to the presence of defects, and such a formed oxide is characterized by conductivity similar to superionic conductors. However, the difference lies in the rapid mixing of particles and vacancies due to the thermal effect, and therefore "short-lived" conductivity occurs in oxides.

The temperature at which high electrical conductivity appears is determined by the Tammann melting point [1, 2, 10, 20]: $(0.5 – 0.8)T_m$ (essentially room temperature, according to Table 2 and Fig. 4, where the first temperature gradient corresponds to the melting of the stainless steel surface), at which surface diffusion begins to transform into bulk diffusion. It is at this temperature that significant interaction between oxides and carbon occurs. All components of the carbon that make up the perovskite will participate in this conductivity.

4. Conclusion

In this article, we analyzed the structural features of high-entropy alloys with laser-induced dendritic structures using topological laser thermodynamics approaches and models of surface laser structures of various configurations. The laser methods for influencing the material surface with the implementation of inhomogeneous dendritic/fractal structures were considered. As a result, existing approaches for considering thermophysical processes

in such topological structures were briefly analyzed. The diffusion processes and implementation of inhomogeneous topological structures of various configurations on the material surface with the formation of dendrites in a laser experiment were simulated. When examining the effects of laser thermodynamics of HEA systems, we estimated the numerical values of the thermodynamic parameters in nanostructured samples, in contrast to the values for tabulated bulk samples. Details of calculations based on the various algorithms used were provided. This makes it possible to mathematically model the electrical properties of dendritic structures using a nanocluster/island nanofilm model, estimating the local field enhancement in the resulting dendritic structures. The analysis and estimated calculations presented in this paper, taking into account the thermodynamic conditions and criteria for the existence of HEA, specifically the ranges of numerical values of entropy and enthalpy, differences in the mole fractions of elements, and latent heats of fusion, suggest the possibility of a perovskite-like high-entropy compound and its martensitic transformation. This requires further verification in future studies.

5. Supplementary Materials

https://disk.yandex.ru/i/zkKkS1WLVHZkUw

6. Conflict of interest

The authors declare no conflict of interest.

References

1. Panchenko VYa. *Laser technologies of materials processing: modern problems of fundamental research and applied developments*. Moscow: FIZMALIT; 2009. 664 p. (In Russ.)
2. Grigor′yants AG, Shiganov IN, Misyurov AI. *Technological processes of laser processing: Studies. Handbook for universities*. Moscow: BMSTU Publ. House; 2006. 664 p. (In Russ.)
3. Römer GRBE, Huis In ’T Veld AJ. Matlab laser toolbox. *Physics Procedia*. 2010;5:413-419. DOI:10.1016/j.phpro.2010.08.068
4. Kandidov VP, Chesnokov SS, Shlenov SA. *Discrete Fourier transform. Study guide*. Moscow: Lomonosov MSU Publ. House; 2019. 88 p. (In Russ.)
5. Bukharov DN, Osipov AV, Arakelyan SM, Kucherik AO. Graph-analytical model of the electrical conductivity of a semiconductor island plumbum telluride nanofilm. *Journal of Physics: Conference Series*. 2019; 1331:012008. DOI:10.1088/1742-6596/1331/1/012008
6. Arakelyan SM, Khudaberganov TA, Istratov AV, Osipov AV, Khor′kov KS. Topological laser-induced quantum states in nanocluster structures: fundamental effects and possible applications (electrophysics and optics). *Optika i spektroskopiya = Optics and Spectroscopy*. 2019;127(7):125-136. (In Russ.)
7. Garnov SV, Abramov DV, Bukharov DN, Khudaiberganov TA, et al. Electrophysics of carbon 1d structures obtained in a laser experiment: models and demonstration. *Uspekhi Fizicheskih Nauk = Physics-Uspekhi*. 2024;194(2):115-137. DOI:10.3367/UFNr.2023.12.039620 (In Russ.)
8. Bukharov DN, Tumarkina DD, Kucherik AO, Tkachev AG, et al. Structure control of metal-carbon composites with different nanotopological configurations and electrical conductivity characteristics in a laser experiment. *Journal of Advanced Materials and Technologies*. 2024;9(3):207-235. DOI:10.17277/jamt.2024.03.pp.207-235
9. Bukharov DN, Kucherik AO, Arakelian SM. Nanocluster fractal electrical conductivity in thin films on a solid surface: dimensional model of different configurations and demonstration of results in a laser experiment. *Journal of Advanced Materials and Technologies*. 2023;8(3):227-251. DOI:10.17277/jamt.2023.03.pp.227-251
10. Trakhtenberg LI, Mel′nikova MYa. *Metal/semiconductor containing nanocomposites*. Moscow: Technosphere; 2019. 624 p. (In Russ.)
11. Arakelyan SM, Kucherik AO, Prokoshev VG, Rau VG, Sergeyev AG. *Introduction to femtonanophotonics: fundamental principles and laser methods for the controlled production and diagnosis of nanostructured materials: a textbook*. Moscow: Logos; 2020. 744 p. (In Russ.)
12. *Practical recommendations for the development of printed circuit boards*. Available from: https://btpit36.ru/pluginfile.php/5733/mod_resource/content/2/samspcbguide_ce_1.1.pdf [Accessed 21 June 2025]
13. Shumilin AV, Bel′tyukov YaM. The effect of nonequilibrium correlations on the effective resistance between centers in the theory of hopping conduction. *Fizikat verdogo tela = Physics of the Solid State*. 2019; 61(11):2116-2121. DOI:10.21883/FTT.2019.11.48416.509 (In Russ.)
14. Kuvayskova YuE. *Algorithms of discrete mathematics: a textbook*. Ulyanovsk: UlGTU Publ. House; 2017. 99 p. ISBN 978-5-9795-1635-6 (In Russ.)
15. Korchagin SA, Terin DV, Klinayev YuV. Modeling of a fractal composite and investigation of its electrical characteristics. *Matematicheskoye modelirovaniye i chislennyye metody*. 2017;13(1):22-31. (In Russ.)
16. Bonch-Bruyevich VL. Problems of the electron theory of disordered semiconductors. *Uspekhi fizicheskikh nauk = Physics-Uspekhi*. 1983;140(4):583-637. DOI: 10.3367/UFNr.0140.198308b.0583 (In Russ.)
17. Cao M, Chen J, Sun X, Xie F, Li B. Theoretical predictions and experimental verifications of SERS detection in colorants. *RSC Advances*. 2023;13(22):15086-15098. DOI: 10.1039/D3RA01584J

18. *Detecting and identifying food colorants with SERS. Spectroscopy online*. Available from: https://www.spectroscopyonline.com/view/detecting-and-identifying-food-colorants-sers [Accessed 21 June 2025]

19. Tkachenko LA, Repina AV. *The theory of unsteady heat transfer: A textbook*. Kazan: Kazan University Publ. House; 2017. 139 p. (In Russ.)

20. Rykalin NN, Uglov AA, Zuyev IV, Kokora AN. *Laser electron beam processing of materials: A reference book*. Moscow: Mashinostroyeniye; 1985. 496 p. (In Russ.)

21. Libenson MN, Yakovlev EB, Shandybina GD. *Interaction of laser radiation with matter (power optics). Part II. Laser heating and destruction of materials. Study guide*. Saint-Petersburg: ITMO Publ. House; 2014. 181 p. (In Russ.)

22. Antonov DN, Burtsev AA, Butkovskiy OYa. Distribution of dendrites produced on the surface of steel as a result of exposure to laser radiation. *Zhurnal tekhnicheskoy fiziki = Technical Physics*. 2016;86(1):110-115. (In Russ.)

23. Unutulmazsoy Y, Merkle R, Fischer D, Mannhart J, Maie, J. The oxidation kinetics of thin nickel films between 250 and 500 °C. *Physical Chemistry Chemical Physics*. 2017;19(13):9045-9052. DOI:10.1039/C7CP00476A

24. Vorobev AH. *Diffusion problems in chemical kinetics. Study guide*. Moscow: Lomonosov MSU Publ. House; 2003. 98 p. (In Russ.)

25. AISI 304 *Stainless steel characteristics*. Available from: https://inoxtrade.ru/info/commoninfo/item100590/aisi-304/ [Accessed 21 June 2025]

26. *Special functions*. Available from: https://www.tutorialspoint.com/python/special_functions.htm [Accessed 21 June 2025]

27. Sergeyev NA, Ryabushkin DS. *Physics of nanosystems: monograph*. Moscow: Logos; 2016. 192 p. (In Russ.)

28. Borlakov KhSh, Kochkarova PA. Fractal dimension as a thermodynamic parameter. *Izvestiya vuzov. Severo-Kavkazskiy region. Yestestvennyye nauki*. 2006;3:50-52. (In Russ.)

29. Aleshin MP, Tumarkina DD, Oparin ES, Bukharov DN, et al. Models and structures in the electrophysics of high-entropy alloys with laser-induced fractal surface objects. *Physics of Metals and Metallography*. 2024;125(9):970-985. DOI:10.1134/S0031918X24601574

30. Suzdalev IP. *Nanotechnology: Physico-chemistry of nanoclusters, nanostructures and nanomaterials*. Moscow: LIBROKOM Publ. House; 2019. 592 p. (In Russ.)

31. Tumarkina DD, Butkovskiy OY, Bolachkov AV, Burtsev AA. Surface topology of mixing entropy resulting from two-pulse laser ablation of stainless steel. *Fiziko-khimicheskie aspekty izucheniya klasterov, nanostruktur i nanomaterialov*. 2023;15:869-878. DOI:10.26456/pcascnn/2023.15.869 (In Russ.)

32. Rekhviashvili SH, Kishtikova EV. On the melting temperature of nanoparticles and nanostructured substances. *Pis'ma v zhurnal tekhnicheskoy fiziki = Technical Physics Letters*. 2006;32(10):50-55. (In Russ.)

33. *Atomic radii*. Available from: https://dpva.ru/Guide/GuidePhysics/Length/AtomicRadius [Accessed 21 June 2025]

34. Spivak LV, Shchepina NE. Polymorphic transformations in iron and zirconium. *Technical Physics*. 2020;65:1100-1105. DOI:10.1134/S1063784220070221

35. Pochtenny AE. *Jump conductivity under direct current in intrinsic and doped organic semiconductors: monograph*. Minsk: BGTU Publ. House; 2016. 171 p. (In Russ.)

36. Blinova NA, Filippov MV. Method of finding a path in a labyrinth in the presence of interference. *Novyye informatsionnyye tekhnologii v avtomatizirovannykh sistemakh*. 2019;22:46-50. (In Russ.)

37. Krevchik VD, Semenov MB, Krevchik PV. Quantum tunneling with dissipation: an application to tunnel transport for semiconductor quantum dots in a combined AFM / STM system under external electric field conditions (review). Part II. *Izvestiya vysshikh uchebnykh zavedeniy. Povolzhskiy region. Fiziko-matematicheskie nauki*. 2020;(4):132-185. DOI:10.21685/2072-3040-2020-4-9 (In Russ.)

38. Simonyan ES, Medvedeva OA, Medvedev SN. Creation of maze with multiple solutions, search for all solutions and editing them. *Modelirovaniye, optimizatsiya i informatsionnyye tekhnologii*. 2019;7(2(25)):365-381. DOI:10.26102/2310-6018/2019.25.2.030 (In Russ.)

39. Krasnov ES. Methodology for evaluating path-finding algorithms in a maze to select a mobile robot movement strategy. *Izvestiya Tul'skogo gosudarstvennogo universiteta. Tekhnicheskiye nauki*. 2012;11(2):179-187. (In Russ.)

40. Moskalev PV. Analysis of the structure of a percolation cluster. *Zhurnal tehnicheskoy fiziki = Technical Physics*. 2009;79(6):1-7. (In Russ.)

41. Moshnikov V.A., Nalimova S.S., Seleznev B.I. Gas-sensitive layers based on fractal-percolation structures. *Semiconductors*. 2014;48(11):1499-1503. DOI:10.1134/S1063782614110177

42. Montaldi J, Smolyanov OG. Feynman path integrals and Lebesgue–Feynman measures. *Doklady Mathematics*. 2017;96(1):368-372. DOI:10.1134/S1064562417040226

43. Tsitsiashvili GSh, Osipova MA, Losev AS. Derivation of asymptotic constants for the disconnection probability of a planar weighted graph. *Prikladnaya diskretnaya matematika*. 2014;2:97-100. (In Russ.)

44. Kuznetsov VM, Khromov VI. Fractal representation of the Debye theory for studying the heat capacity of macro-and nanostructures. *Technical Physics*. 2008; 53(11):1401-1406. DOI:10.1134/S1063784208110029

45. Goryachev NS, Kukushkin VI, Belik AY, Rybkin AY, et al. Using SERS and SEF spectroscopy to detect fullerene-dye dyads in water and biological structures. *Bulletin of the Russian Academy of Sciences: Physics*. 2022;86(4):418-422. DOI:10.3103/S1062873822040116

Information about the authors / Информация об авторах

Darya D. Tumarkina, Teaching Assistant, Vladimir State University (VlSU), Vladimir, Russian Federation; ORCID 0009-0007-5496-4234; e-mail: tumarkina.darya@mail.ru

Oleg Ya. Butkovsky, D. Sc. (Phys. and Math.), Professor, VlSU, Vladimir, Russian Federation; ORCID 0000-0001-6052-666X; e-mail: OYButkovskiy@fa.ru

Dmitry N. Bukharov, Cand. Sc. (Phys. and Math.), Associate Professor, VlSU, Vladimir, Russian Federation; ORCID 0000-0002-4536-8576; e-mail: buharovdn@gmail.com

Irina V. Burakova, Cand. Sc. (Eng.), Associate Professor, Tambov State Technical University (TSTU), Tambov, Russian Federation; ORCID 0000-0003-0850-9365; e-mail: iris_tamb68@mail.ru

Alexander E. Burakov, Cand. Sc. (Eng.), Associate Professor, Acting Head of the Department, TSTU, Tambov, Russian Federation; ORCID 0000-0003-4871-3504; e-mail: m-alex1983@yandex.ru

Sergey M. Arakelian, D. Sc. (Phys. and Math.), Professor, Independent Researcher, Vladimir, Russian Federation; ORCID 0000-0002-6323-7123; e-mail: arak@vlsu.ru

Тумаркина Дарья Денисовна, ассистент, Владимирский государственный университет имени А. Г. и Н. Г. Столетовых (ВлГУ), Владимир, Российская Федерация; ORCID 0009-0007-5496-4234; e-mail: tumarkina.darya@mail.ru

Бутковский Олег Ярославович, доктор физико-математических наук, профессор, ВлГУ, Владимир, Российская Федерация; ORCID 0000-0001-6052-666X; e-mail: OYButkovskiy@fa.ru

Бухаров Дмитрий Николаевич, кандидат физико-математических наук, доцент, ВлГУ, Владимир, Российская Федерация; ORCID 0000-0002-4536-8576; e-mail: buharovdn@gmail.com

Буракова Ирина Владимировна, кандидат технических наук, доцент, Тамбовский государственный технический университет (ТГТУ), Тамбов, Российская Федерация; ORCID 0000-0003-0850-9365; e-mail: iris_tamb68@mail.ru

Бураков Александр Евгеньевич, кандидат технических наук, доцент, и. о. заведующего кафедрой, ТГТУ, Тамбов, Российская Федерация; ORCID 0000-0003-4871-3504; e-mail: m-alex1983@yandex.ru

Аракелян Сергей Мартиросович, доктор физико-математических наук, профессор, независимый исследователь, Владимир, Российская Федерация; ORCID 0000-0002-6323-7123; e-mail: arak@vlsu.ru

Received 21 August 2025; Revised 04 October 2025; Accepted 10 October 2025